Full Paper ELECTROANALYSIS

Electrical and Sensing Properties of Single-Walled Carbon Nanotubes Network: Effect of Alignment and Selective Breakdown

Jae-Hong Lim, a Nopparat Phiboolsirichit, Syed Mubeen, Youngwoo Rheem, Marc A. Deshusses, Ashok Mulchandani, Nosang V Myung *

^a Department of Chemical and Environmental Engineering and Center for Nanoscale Science and Engineering, University of California-Riverside, Riverside, CA 92521, USA

*e-mail: myung@engr.ucr.edu

Received: June 18, 2009 Accepted: August 16, 2009

Abstract

The electrical transport and NH_3 sensing properties of randomly oriented and aligned SWNT networks were presented and discussed. The results indicate that aligned SWNT-FETs have better FET characteristics due to the reduced number of interconnected nodes. This was particularly true as the resistance of the devices increased. Gated electrical breakdown was implemented to selectively remove metallic (m-) SWNTs, thereby reducing scattering centers. This technique provided significant improvements in FET characteristics resulting in greater on/off ratio (e.g. 10^4). AC dielectrophoretic alignment followed by selective electrical breakdown of m-SWNTs can significantly enhance the semiconducting properties of SWNT networks which resulted in highly sensitive sensors.

Keywords: SWNT, Field effect transistor, Alignment, Ammonia, Sensors, Nanotubes

DOI: 10.1002/elan.200900314

1. Introduction

Carbon nanotubes have many potential applications in a wide array of fields such as nanoelectronics, field emitters, sensors, displays, hydrogen storage, batteries, polymer matrix composites, and nanoscale reactors [1–4]. Among these applications, the single-walled carbon nanotube based field effect transistor (SWNT-FET) is one of the most promising candidates for next generation electronics and sensors because of its unique electrical properties [1]. Typically, two different configurations (i.e. single SWNT and SWNT network based device) have been utilized in SWNT-FET where SWNTs act as carrier channels between the source and drain. Although excellent electronic transport properties have been demonstrated in SWNT, reproducible manufacturing and cost effective integration remain important challenges for advancing the field.

Direct manipulation of SWNTs, for instance with atomic force microscope (AFM) tips, is the most well-controlled method to create single SWNT-based devices. However, it is time-consuming and not suitable for mass production. Direct growth offers nearly the same degree of positioning but requires specialized materials and pattering techniques [5–7]. Drop casting of SWNT solutions or suspensions combined with alternating current (AC) or direct current (DC) dielectrophoresis has attracted interest due to the relative simplicity by which individual as well as networks of SWNT can be assembled on prefabricated microelectrodes [8]. A relatively good control of the number of SWNTs

bridging the electrodes can be obtained by adjusting the shape and dimension of electrodes and the concentration of SWNT in solution. DC electric field assisted alignment typically results in deposition of nanotubes or nanoparticles on the positive electrode with a limited number of nanotubes aligned across the electrodes as a consequence of mechanical flow by electroosmotic [9] and electrohydrodynamic interactions [10]. However, AC electric fields have proven to be effective for aligning CNTs nearly perpendicular to electrodes, mitigating nanotube deposition and even detangling nanotubes depending on the AC frequency [11]. Compared to single SWNT-based devices, SWNT networkbased devices have the advantage of a more homogeneous behavior. However, SWNT networks suffer from the fact that they will usually be made of both metallic (m-) and semiconducting (s-) SWNTs due to the different chiralities obtained during SWNT synthesis. s-SWNTs with a high on/ off current ratio are necessary for transistors, whereas m-SWNTs are required for interconnects. Preferential breakdown of m-SWNTs in a SWNT network can be accomplished by applying a high voltage across the electrodes, while majority carriers for the s-SWNTs are depleted by applying a high gate voltage [12].

In this study, we utilized two different techniques (i.e. drop-casting and AC dielectrophoresis alignment) to fabricate randomly oriented and aligned SWNT networks based FETs and sensors. The effect of alignment techniques on electrical transfer characteristics and gas sensing performance were systematically investigated. The morphologies



^b Department of Civil and Environmental Engineering, Box 90287, Duke University, Durham, NC 27708, USA

Full Paper J. Lim et al.

of assembled networks were determined using scanning electron and atomic force microscope. In addition, the electrical breakdown technique was employed to selectively eliminate m-SWNTs and its effect on electrical and sensing properties was also investigated.

2. Experimental

2.1. Materials and Substrates

The caboxylated SWNTs (SWNT-COOH 80–90% purity, bundle length: ~1 µm, bundle diameter: 4–5 nm) were purchased from Carbon Solution, Inc. (Riverside, CA). The nanotubes (1 mg/mL) were ultrasonically dispersed in N, N-dimethylformamide (DMF) and the suspension was centrifuged at $31,000 \times g$ for 90 min to remove the insoluble fraction and aggregates. Detailed SWNT solution preparation procedure is described in our previous work [13]. Substrates were prepared by atomic layer deposition (Savannah 100, Cambridge Nanotech) of HfO₂ (L_{ox} = 250 nm) on highly doped p-type Si substrates. Ti/Au (20/180 nm) microelectrodes were fabricated on HfO₂/Si substrates using standard lift-off techniques where the width (W) and gap (L_{SD}) of the electrodes was 200 µm and 3 µm, respectively.

2.2. Preparation of SWNT FETs

Two different SWNT network samples were prepared: randomly oriented and aligned. Randomly oriented SWNT-FET samples were fabricated by dropping 0.2 µL of the nanotube suspension onto the prefabricated microelectrodes in the absence of an electric field. For aligned samples, a 0.2 μL drop of the nanotube suspension was deposited onto the prefabricated microelectrodes followed by applying AC dielectrophoretic field of $V_{\rm rms} = 0.36 \, {\rm V}$ at $f = 4 \, {\rm MHz}$. The alignment time was varied from 2 to 10 s to obtain desired electrical resistance. After assembly, the devices were rinsed with deionized water, dried by gently blowing nitrogen gas and annealed at 300 °C for 1 h under reducing environments (5% hydrogen in nitrogen) to improve the contact between the SWNT network and the electrodes and to remove residue from solution. The electrical resistance of SWNT-FETs was adjusted by controlling alignment time.

To further improve the electrical transport characteristics, the selective removal of metallic nanotubes in aligned SWNT-FETs by electrical breakdown was investigated [12]. The principle of this technique was to burn/oxidize metallic SWNTs preferentially by producing high current in them to generate heat while eliminating or minimizing the current flow in p-type semiconducting SWNTs. This was achieved by applying a 20 V gate voltage while increasing source-drain potential ($V_{\rm DS}$) during consecutive sweeps with increasing voltage ranges.

2.3. Characterizations

The temperature dependent current – voltage (I-V) characteristics for the fabricated devices were measured using a Keithley source-measure unit (Model 236). Operating temperature was varied from 30 to 273 K using cold-finger cryogenic system (Janis CCS-350SH). Activation energies $(E_{\rm A})$ were calculated from electrical resistance Arrhenius plots in the temperature region above 70 K. The SWNT field-effect transistors were formed by using the highly doped silicon substrate as a back gate. The electronic measurements were performed using two Keithley sourcemeasure units in ambient environments. The surface morphology of SWNT-FETs was examined using a field emission scanning electron microscope (SEM, Philips XL30 FEG) and an atomic force microscope (Innova, Veeco Instruments Inc.) in order to determine distribution of SWNTs. In addition, line scans were conducted by standard tapping mode AFM for the height of SWNT bundles histogram analysis.

3. Results and Discussion

3.1. Morphology Characterization of SWNT-FETs

Figure 1 shows the SEM images of randomly oriented and aligned SWNT-FETs. The drop cast SWNTs networks had no preferential orientation with many SWNTs interconnections existing within the electrode gap. On the other hand, samples subjected to AC dielectrophoresis consisted of SWNTs aligned perpendicularly to the electrodes.

Figure 2 reports the height distributions of randomly oriented and aligned SWNT-FETs of low ($<\!10\,k\Omega$) and high ($>\!1\,M\Omega$) resistance ranges, respectively. As the resistance of the networks increased, i.e., the density of SWNTs decreased, a distinct shift in the height distribution towards smaller diameter is observed, indicating that small bundles are preferentially deposited in a short time. The prolonged alignment time can attract large bundles, resulting in the decrease in the resistance and height distribution shift toward larger diameter.

3.2. Activation Energy Characterization of SWNT-FETs

Activation energies (E_A) of randomly oriented and aligned SWNTs networks of different resistances are compared in Figure 3a. In the case of randomly oriented SWNTs, E_A increased by only 3.3 fold as the resistance increased from 2.2 k Ω to 1.7 M Ω . On the other hand, E_A of aligned samples showed a much greater dependency with resistance and increased by 17.3 fold. The reported E_A of a single m-SWNT and a s-SWNT are 5 and 29 meV, respectively [14]. Here, the E_A of randomly oriented and aligned samples of less than 10 k Ω (i.e., dense networks) resistances were 6.6 and 5.1 meV, respectively. It might be inferred that low resistance samples might have large bundles containing large

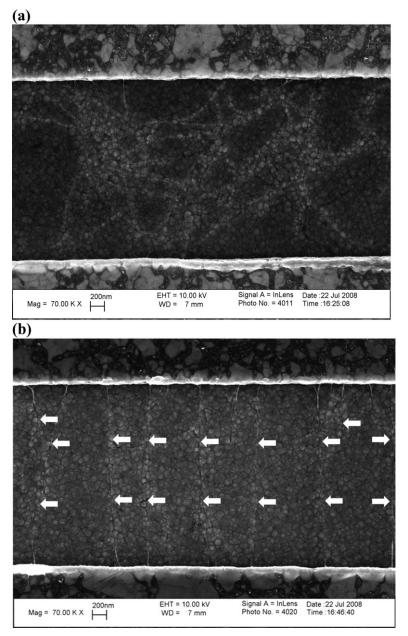


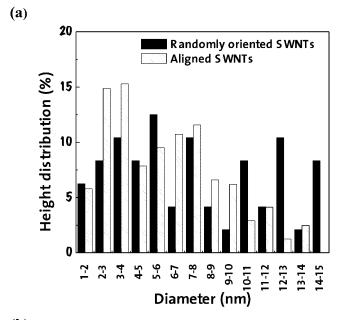
Fig. 1. SEM images of (a) randomly oriented and (b) aligned SWNT-FETs prepared by applying alternating current of $0.36\ V_{\rm rms}$ at a frequency of 4 MHz. The position of SWNTs is indicated by arrows.

portion of m-SWNTs, resulting in that the current in both samples flows mostly through m-SWNTs. This is in sharp contrast with $E_{\rm A}$ values of 22.0 and 88.3 meV, respectively, of randomly oriented and aligned samples above 1 M Ω (i.e., sparse networks). In the latter case, the Schottky barrier height might also contribute to $E_{\rm A}$, possibly accounting for the drastic increase of $E_{\rm A}$ as the total resistance is the sum of contact and sample resistances. Figure 3b shows a histogram of the height distribution of three aligned SWNT-FETs ranging from 9.6 k Ω to 3.0 M Ω , indicating that the fraction of small diameter SWNT bundles in the devices is a direct function of the resistance. Based on these results, high $E_{\rm A}$ of highly resistive aligned SWNT-FETs can be attributed to more deposition of s-SWNTs containing small bundles.

3.3. FET Characterization of SWNT-FETs

The transfer characteristics of randomly oriented and aligned samples of low (i.e. 6.3 and $5.9 \, \mathrm{k}\Omega$) and high resistance (i.e. 154 and $294 \, \mathrm{k}\Omega$) are plotted in Figure 4. The higher resistance aligned FET clearly exhibited an off-state and a stronger dependency on the gate bias. These results infer more semiconducting properties as the resistance for aligned samples increases. This is also supported by the comparison of E_A shown in Figure 3a, which shows s-SWNTs are more predominant as the resistance increases.

Figure 5 shows the dependency of carrier concentration and field effect mobility on the resistance of aligned and randomly oriented SWNTs. The carrier concentration and



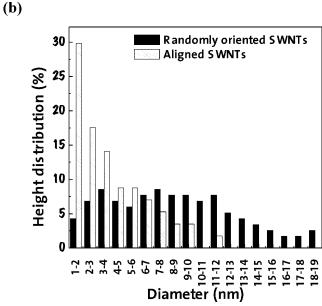


Fig. 2. Comparison of histogram from randomly oriented and aligned SWNT-FETs at (a) low resistance (8.8 and 9.6 k Ω , respectively) and (b) high resistance (1.8 and 3.0 M Ω , respectively).

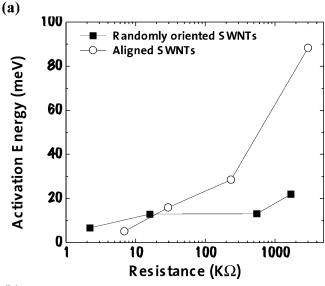
field effect mobility were calculated using following equations:

$$p = C_{\rm G} V_{\rm G,T} / e L_{\rm SD} \tag{1}$$

$$\mu = L_{\rm SD}^2 \, \left(\frac{\mathrm{d}I}{\mathrm{d}V} \right) / C_{\rm G} V_{\rm D} \tag{2}$$

$$C_{\rm G} = \varepsilon W L_{\rm SD} / L_{\rm ox} \tag{3}$$

where p is the hole carrier concentration, C_G the approximate capacitance, $V_{G,T}$ the threshold voltage to deplete the SWNTs, μ the field effect carrier mobility, V_D the drain voltage, and ε the dielectric constant of HfO₂ [15]. The



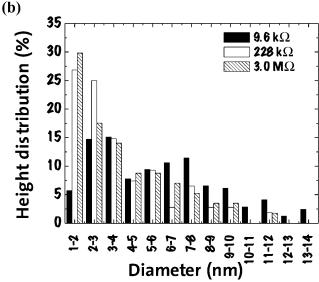


Fig. 3. (a) Thermal activation energy and (b) histogram for randomly oriented and aligned SWNT-FETs of different electrical resistances.

transconductance of dI/dV was determined from each transfer characteristics in the linear regime to calculate μ . The value of C_G slightly overestimates the gate capacitance and therefore underestimates the carrier mobility and overestimate the carrier concentration due to the lower fill factor [16]. However, the comparison of carrier mobilites and carrier concentrations can be done. The carrier concentrations of aligned samples were in the range of 10¹⁰ to 1011 cm⁻¹ without apparent trend with the resistance. This contrasts with the linear trend obtained for randomly oriented SWNTs, which may be the result of the increased number of interconnected nodes in the low resistance samples, which easily trap charge carriers. Figure 5b shows that carrier mobility in aligned samples was higher than that in randomly oriented samples of the same resistance over the entire resistance range. Randomly oriented samples were expected to have higher carrier mobilities than aligned

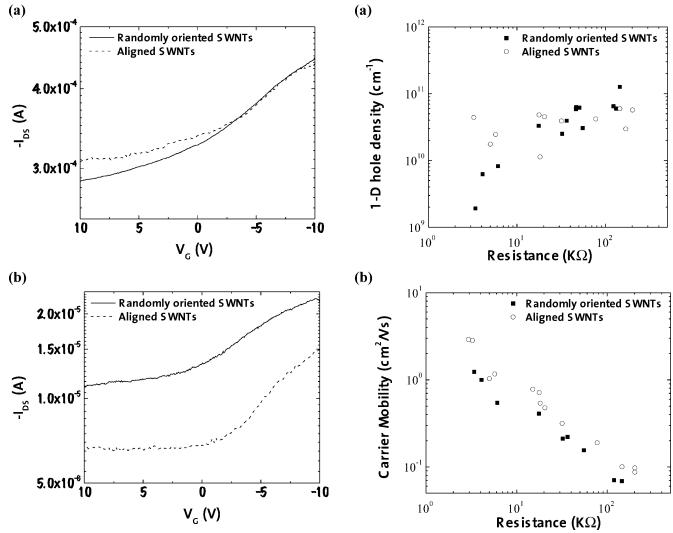


Fig. 4. Transfer characteristics of FETs made of networks of randomly oriented and aligned SWNTs: (a) low resistance (6.3 and 5.9 k Ω , respectively) and (b) high resistance (154 and 294 k Ω , respectively).

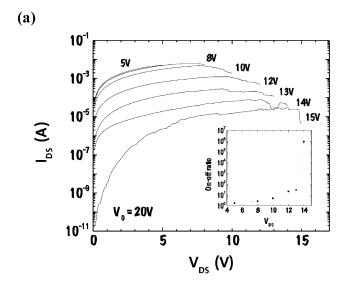
Fig. 5. Carrier concentration (a) and field effect mobility (b) of randomly oriented and aligned SWNT-FETs as a function of the electrical resistance.

samples because actual electrically conducting channel lengths exceed the electrode gap length (Fig. 1). This behavior is due to a relatively small fraction of the applied source-drain voltage drop over the parasitic contact resistance in long channel FETs, as compared to short channel FETs [17]. However here, randomly oriented samples had lower carrier mobility than aligned samples, most probably because the interconnected nodes acted as interface defects, either trapping or scattering carriers. These nodes, which are in lower density in aligned samples, could be a dominant factor in determining the carrier mobility.

3.4. Breakdown Process of m-SWNTs

Figure 6a shows $I_{\rm DS}-V_{\rm DS}$ characteristics for the successive breakdown events which resulted in a partial conductance drop with each breakdown event. The most important drop occurred near 12 V in the 14 V breakdown curve where the

current appears to saturate near 30 µA and saturate again at 55 μA at higher voltage after abruptly increasing. This increase in current-carrying capacity indicates that the number of conducting channels within the bundle increased. This is only possible if additional channels of metallic SWNTs within the bundle are made, which were not originally contacted by source and drain electrodes. The inset of Figure 6a provides additional support, illustrating the steady on-off ratio increase with increasing V_{DS} up to 13 V (with 20 V of V_G), indicating that additional current paths were created during the breakdown process. However, the data indicate that there are mostly semiconducting SWNTs left after applying 15 V between the drain and the source as the on-off ratio increased by five orders of magnitude. Figure 6b shows the I_{DS} dependency with V_G for the FETs with 2 V of $V_{\rm DS}$ after each breakdown cycle, which indicates that I_{DS} modulation is amplified as the breakdown voltage increases with more than a 10⁴ on-off ratio. Figure 7 shows the comparison of carrier concentration and field Full Paper J. Lim et al.



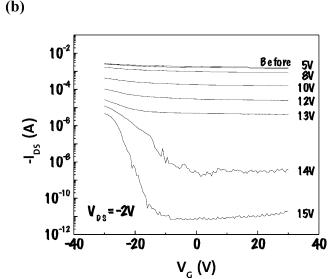
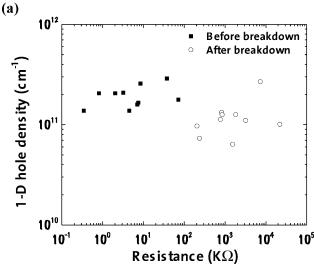


Fig. 6. (a) $I_{\rm DS}$ vs. $V_{\rm DS}$ during metallic SWNTs breakdown at $V_{\rm G}$ of 20 V. Inset shows on-off ratio after each breakdown voltage. (b) $I_{\rm DS}$ vs. $V_{\rm G}$ after each breakdown cycle showing selective metallic SWNT breakdown after $V_{\rm DS}$ reached 15 V.

effect carrier mobility of aligned SWNT-FETs before and after breakdown of the metallic SWNTs. The carrier concentration after breakdown decreases due to the elimination of metallic SWNTs and carrier mobility increases due to the lack of the scattering centers resulting from the carriers.

3.5. Sensing Properties of SWNT-FETs

Figure 8 shows the electrical transfer characteristics of aligned SWNT before (a) and after (b) the electrical breakdown process in the presence of different NH₃ concentrations. Since the sensing mechanism for NH₃ on SWNTs is based on a charge transfer between the electron-donating NH₃ molecules and the s-SWNTs, the carrier



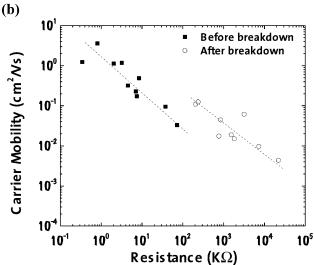
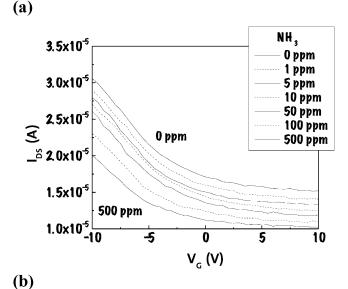


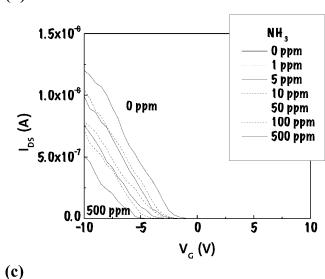
Fig. 7. Carrier concentration (a) and field effect mobility (b) of aligned SWNT-FETs before and after metallic SWNTs breakdown depending on resistance.

concentration of SWNT network decreased upon absorption of NH_3 [18]. Compared to aligned SWNT networks before the electrical breakdown of m-SWNTs, aligned SWNT network after the electrical breakdown show a dramatic change in the electrical transfer characteristics upon exposure to NH_3 including shifts of the threshold voltage ($V_{G,T}$) to the lower voltage with the increase in the concentration of NH_3 . These dramatic changes in the electrical transfer characteristics allow to tune the sensitivity toward NH_3 by adjusting the gate voltage (Fig. 8C).

4. Conclusions

Randomly oriented and aligned SWNT networks based field effect transistors (FETs) were fabricated by means of drop-casting and AC dielectrophoresis alignment techniques, respectively, and their morphology and electron transport and sensing properties were systematically inves-





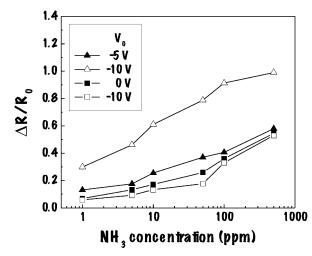


Fig. 8. Transfer characteristics change of SWNT-FETs (a) before and (b) after the breakdown process. (c) The comparison of sensitivity from SWNT-FETs before (\blacksquare) and after (\blacktriangle \triangle) the breakdown process under different V_G .

tigated. The activation energy $(E_{\rm A})$ of dense networks (resistance < $10~{\rm k}\Omega$) of randomly oriented and aligned SWNTs was 6.6 and 5.1 meV, respectively. Conversely, $E_{\rm A}$ of sparse networks (resistance > $1~{\rm M}\Omega$) of randomly oriented and aligned SWNTs was 22.0 and 88.3 meV, respectively. This might be attributed to preferential assembled of semiconducting SWNTs and the increase of Schottky barrier height. The aligned SWNT-FETs showed higher field effect carrier mobilities than randomly oriented SWNT-FETs because of the reduced number of interconnected nodes. Furthermore, the electric breakdown process eliminates metallic-SWNTs thereby enhancing transfer characteristics and sensing performance toward ammonia.

5. Acknowledgements

This material is based on research sponsored by The National Institute of Environmental Health Sciences under agreement number (Grant # U01ES016026).

6. References

- [1] R. H. Baughman, A. A. Zakhidov, W. A. de Heer, *Science* 2002, 297, 787.
- [2] H. Dai, Surf. Sci. 2002, 500, 218.
- [3] T. Zhang, S. Mubeen, N. V. Myung, M. A. Deshusses, Nanotechnology 2008, 332001.
- [4] T. Zhang, M. B. Nix, B.-Y. Yoo, M. A. Deshusses, N. V. Myung, *Electroanalysis* 2006, 18, 1153.
- [5] S. Fan, M. G. Chapline, N. R. Franklin, T. W. Tombler, A. M. Cassell, H. Dai, *Science* **1999**, 283, 512.
- [6] Y. Huang, X. Duan, Q. Wei, C. M. Lieber, Science 2001, 291, 630.
- [7] M. Mauger, V. T. Binh, A. Levesque, D. Guillot, *Appl. Phys. Lett.* 2004, 85, 305.
- [8] M. R. Diehl, S. N. Yaliraki, R. A. Beckman, M. Barahona, J. R. Heath, *Angew. Chem. Int. Ed.* 2002, 41, 353.
- [9] Y. Solomentsev, M. Bohmer, J. L. Anderson, *Langmuir* **1997**, 13, 6058.
- [10] M. Trau, D. A. Saville, I. A. Aksay, Langmuir 1997, 13, 6375.
- [11] M. Senthil Kumar, T. H. Kim, S. H. Lee, S. M. Song, J. W. Yang, K. S. Nahm, E. K. Suh, *Chem. Phys. Lett.* **2004**, 383, 235
- [12] P. G. Collins, M. S. Arnold, P. Avouris, Science 2001, 292, 706.
- [13] S. Mubeen, T. Zhang, B. Yoo, M. A. Deshusses, N. V. Myung, J. Phys. Chem. C 2007, 111, 6321.
- [14] V. Skakalova, A. B. Kaiser, Y. S. Woo, S. Roth, *Phys. Rev. B* 2006, 74, 085403.
- [15] R. Martel, T. Schmidt, H. R. Shea, T. Hertel, P. Avouris, Appl. Phys. Lett. 1998, 73, 2447.
- [16] E. S. Snow, P. M. Campbell, M. G. Ancona, J. P. Novak, *Appl. Phys. Lett.* 2005, 86, 033105.
- [17] S. Luan, G. W. Neudeck, J. Appl. Phys. 1992, 72, 766.
- [18] J. Kong, N. R. Franklin, C. Zhou, M. G. Chapline, S. Peng, K. Cho, H. Dai, *Science* 2000, 287, 622.